5

TrES-1: The transiting planet of a bright K0V star

Los astros despliegan sus órbitas
imposibles. Luego congelan
la luz esclava. Reina el hombre
en el centro del Universo.
José Hierro (*Cuanto sé de mi, 1957)*

We report the detection of a transiting Jupiter-sized planet orbiting a relatively bright (V=11.79) K0V star. We detected the transit light-curve signature in the course of the TrES multi-site transiting planet survey, and confirmed the planetary nature of the companion via multicolor photometry and precise radial velocity measurements. We designate the planet TrES-1; its inferred mass is 0.75±0.07 M_J, its radius is $1.08^{+0.18}_{-0.04}$ R_J, and its orbital period is 3.030065 ± 0.000008 days. This planet has an orbital period similar to that of HD 209458b, but about twice as long as those of the OGLE transiting planets. Its mass is indistinguishable from that of HD 209458b, but its radius is significantly smaller and fits the theoretical models without the need for an additional source of heat deep in the atmosphere, as has been invoked by some investigators for HD 209458b.

5.1 Introduction

Out of the 16 candidates detected in the Lyra field, and described in the previous chapter, T-Lyr0-03507 (renamed TrES-1 from here after) did pass all the tests that were performed to detect false alarms. These included a careful

analysis of the light curve (a search for out of eclipse modulation and a determination of the mean stellar density from the transit shape), high-resolution observations using the AO system at the 4.2 m William Herschel Telescope (Observatorio del Roque de los Muchachos, La Palma, Spain), and relatively low signal-to-noise radial velocity observations. In the next sections we describe the more detailed observations that were carried out on this candidate, that led to the first transiting planet discovered by a wide-field survey.

5.2 The star in the on-line catalogues

Due to the relatively bright nature of the stars observed by the TrES network, there are a number of useful catalogues that can help to constrain the characteristics of the stars in the field. In the case of TrES-1, for instance, the 2MASS catalogue [1] provided a J-K color of 0.48, which suggests a star with late G or early K spectral types (Cox 2000). The Digitized Sky Survey plates showed no bright companions closer than a radius of $20''$ (basically the size of a STARE star image), which could produce a blend case. The AO observations in J and K helped to further constrain the possibility of a close companion, placing a secure limit of no stellar companions within 2 mags of the star, further than $0.3''$ of the star (see Figure 4.29 of the previous Chapter).

The SIMBAD B and V magnitudes of several stars in the field were used as calibrators to measure the B and V magnitudes of the TrES-1 star from the images of the PSST telescope. Johnson's R filter Observations taken at the IAC80, of the star and several Landolt fields (Landolt 1992) at different airmasses were used to measure the R absolute magnitude of the star. These values, together with the information available on the on-line catalogues, are summarized in Table 5.1.

Ignoring interstellar extinction, the observed V magnitude of 11.79 implies a distance to the star of approximately 150 pc. The USNO-B1.0 proper motion of the star is 47 mas/yr (Monet et al. 2003), which results in a transverse velocity of 26 km/s, when combined with the previous distance. This transverse velocity is fairly typical for low-mass field stars in the solar neighborhood.

5.3 Multicolor observations

There are several blending scenarios that might show a color dependance of the transit depth (Chapter 3), that lead us to perform multicolor observations of TrES-1 transits. At the IAC 80 cm telescope, we observed a partial transit (missing the egress) with Johnson V and I filters; at the University of Colorado

[1] http://www.ipac.caltech.edu/2mass/

TABLE 5.1— Parameters for the TrES-1 Parent Star

Parameter	Value
R.A.	$19^h04^m09^s.8$ (J2000.0)
Declination	+36°37'57″ (J2000.0)
R	11.34
V	11.79
B–V	0.78
J	10.294
J–H	0.407
J–K	0.475
Spectrum	K0 V
M_s	0.88 ± 0.07 $M_\odot$
R_s	$0.85^{0.10}_{-0.05}$ $R_\odot$
GSC	02652-01324
2MASS	19040985+3637574
USNO-B1.0 ppm (RA)	-42 mas yr^{-1}
USNO-B1.0 ppm (Dec)	-22 mas yr^{-1}

Sommers-Bausch Observatory (SBO) 61 cm telescope, we observed a full transit with Johnson B and R filters; at the CfA's Fred L. Whipple Observatory (FLWO) 1.2 m telescope, we observed one full and one partial transit with Sloan g, r, and z filters. The PSST telescope also observed four transits in R during the 2004 season. Figure 5.1 displays all of these observations, along with a fit to a model, which we shall discuss bellow.

5.3.1 The IAC-80 observations

As an example of the observations and data reductions carried out by the previous telescopes, in this subsection we describe in detail the observations performed of the TrES-1 system, at the IAC-80 telescope, the nights of 2004 August 29 and 2005 April 19, using Johnson's R filter.

The raw images were taken using a 2x2 binning of the CCD pixels; this allows a faster readout, reducing it a factor of ∼4, from ∼40 seconds to ∼10 seconds. A slight defocus of the image was applied, in order to reduce the effects of changes in the PSF due to atmospheric and instrumental conditions (seeing, temperature changes, flexures in the system), and also the effect of the intrapixel different sensivities of the CCDs (see, e.g. Penny & Leese 1996).

Calibration of the images involved flat-fielding, subtracting the CCD zero

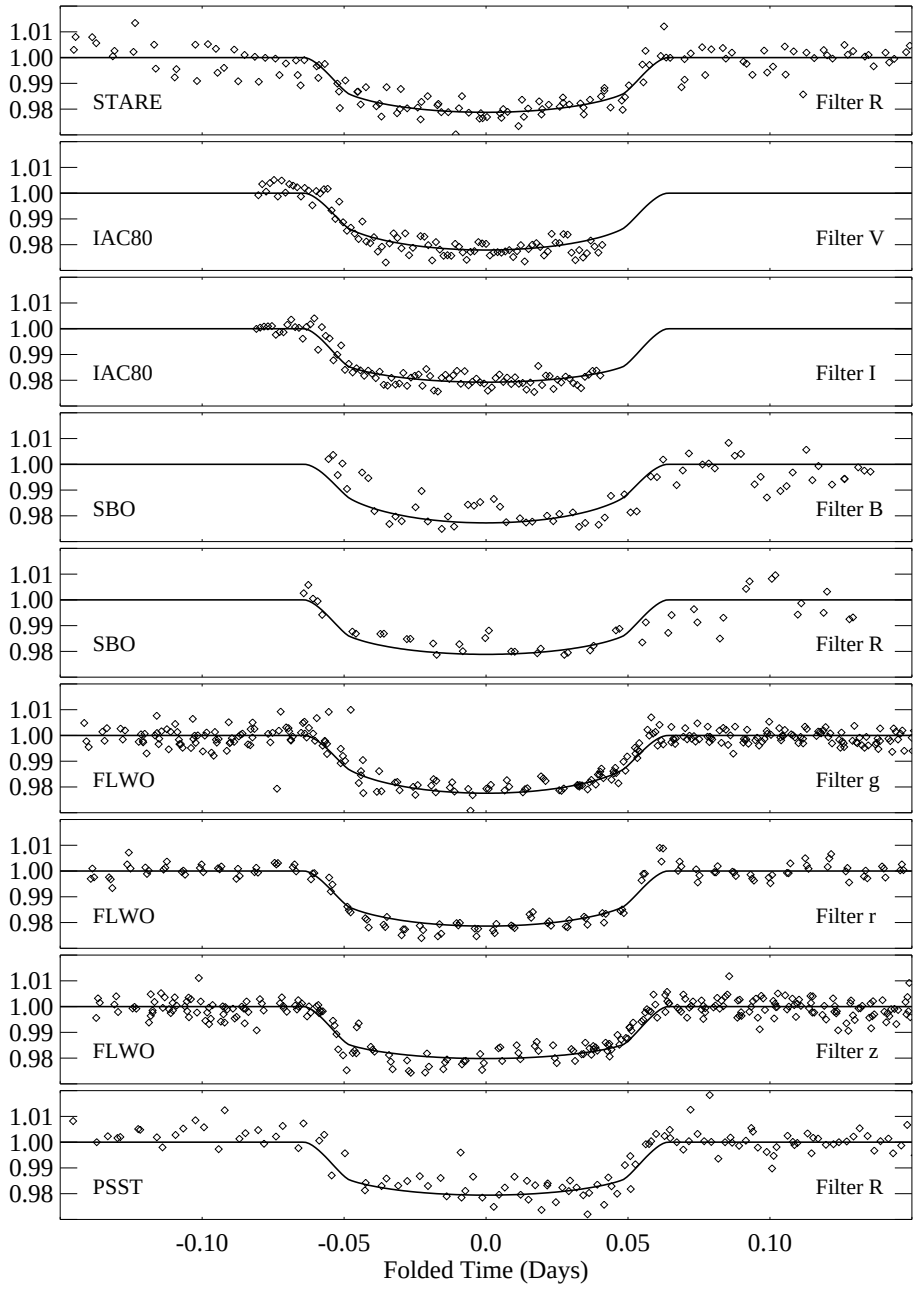

FIGURE 5.1— Time series photometry used in estimating the radius and inclination of TrES-1, plotted against heliocentric time modulo the orbital period from Table 5.2. The telescope and filter bandpass used are indicated on each plot, and discussed in the text. Each set of observations is overplotted with the predicted light curve for that color, given the parameters of Table 5.2

level, using the IRAF's (Tody 1986)[2] CCDPROC routine. All the images were aligned and aperture photometry was performed in the target star and 7 reference stars. The aperture to perform the photometry was allowed to vary, according to changes in the PSF that still were not removed by the defocussing. The typical FWHM of the stars was ∼4 arcsec. Different apertures for each star were chosen in a reference image (brighter stars having bigger apertures), and the ratios between the apertures of the stars were kept constant in every image, varying from image to image by a constant value. This was performed with the Vaphot IRAF routine developed by Deeg & Doyle (2001).

An artificial reference star is then built with the measured instrumental magnitudes of the 7 reference stars. The construction of this average reference star assigns more weight to the brightest stars, for which the photon noise is lower, and thus the dispersion of the points. Visual inspection of the magnitudes of each of the reference stars with the artificial star subtracted allows one to identify variable stars. This variability can be intrinsic of the star, or an instrumental artifact, which can be due to the location of the star close to a dirty part of the CCD which was not completely corrected with the flat-field correction, or confusion due to close fainter stars. Once these variables are identified, they can be removed from the construction of the artificial reference star. For the TrES-1 light curve, three of the seven reference stars were removed from the mean, due to intrinsic variability, or because their inclusion into the mean resulted in a noisier artificial reference star. The Johnson's R light curve, and a 6-points binned light curve is plotted on Figure 5.2. A final light curve in the R filter, sampled in a regular grid of phase points, is plotted in Figure 5.3. The error bars in the binned plots have a total size of the standard deviation of the average divided by the square root of the number of points in the bin.

5.4 Low signal to noise radial velocity observations

This star was observed with the CfA Digital Speedometers (Latham 1992, described in Chapter 3) at seven different epochs spanning 60 days, giving coverage of the full orbital phase. From these exposures, we determined a mean velocity of –20.52 km/s. The average internal error estimate and actual rms achieved were both 0.39 km/s, suggesting that any companion orbiting with a 3.03 day period must have a mass smaller than 5 M_{Jup}. This conclusion is not firm, however, if there is blending light from a third component. Comparisons of our observed spectra with synthetic spectra (calculated by J. Morse using Kurucz models, J. Morse and R.L. Kurucz, private communication), allowed us to estimate that the TrES-1 parent star has T_{eff}=5250±200 K, log$g$=4.5±0.5,

[2]IRAF is distributed by the National Optical Astronomy Observatories.

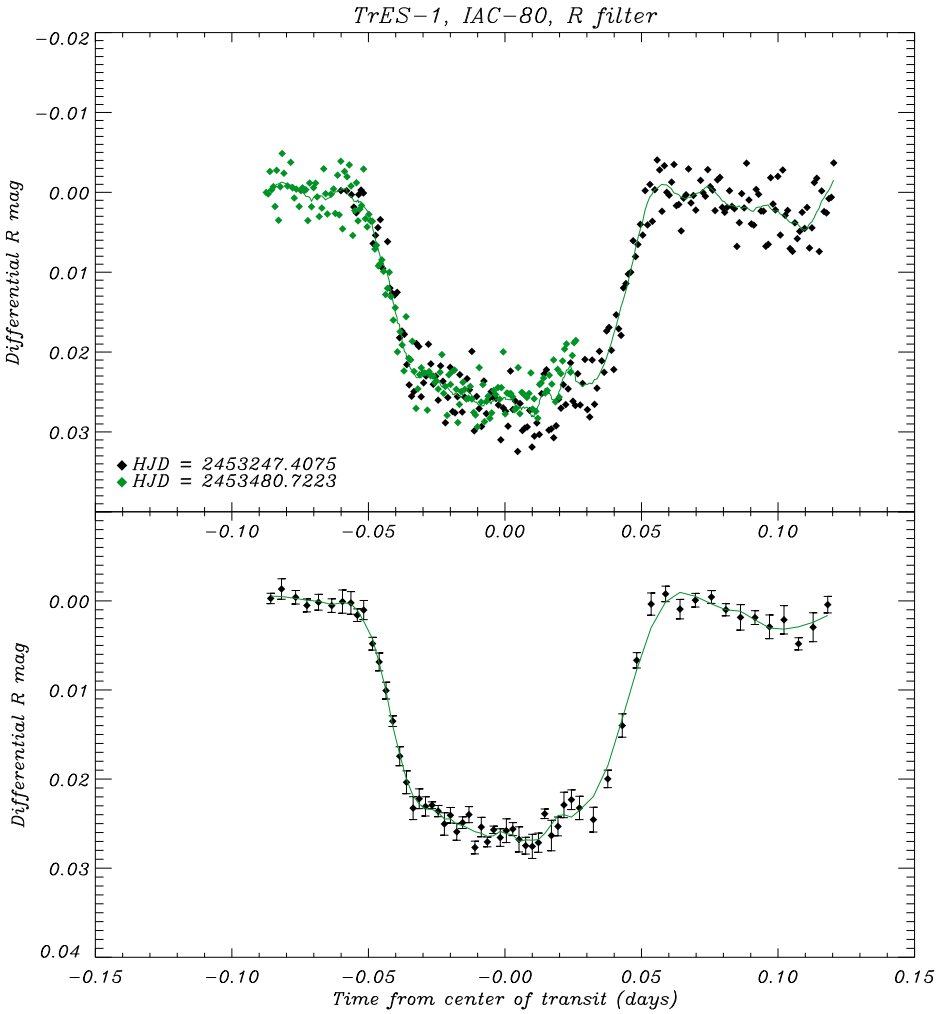

FIGURE 5.2— Top: Light curve of TrES-1 in R filter obtained at the IAC-80 telescope, on two different nights, HJD 2453247 (August 29, 2004) and 2453480 (April 19, 2005). The ephemerides listed in Table 5.2 were used to put the data in phase. Bottom: Same light curve, but averaged in 6 points bins; the error bars are the standard deviation of the average divided by the square root of the number of points in the bin.

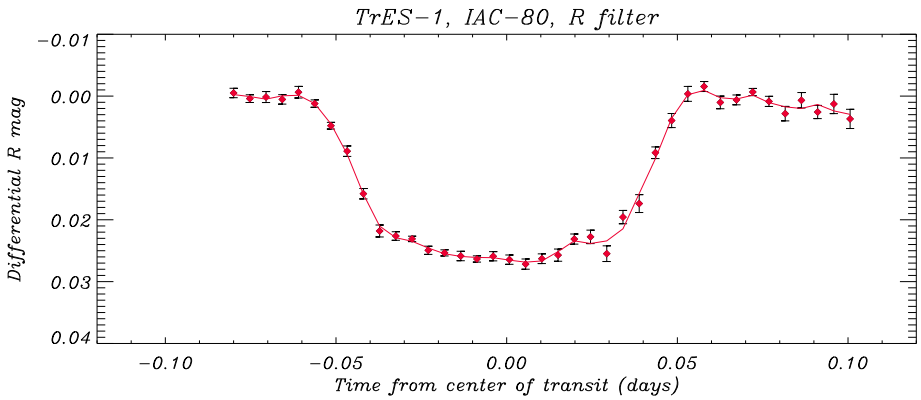

FIGURE 5.3— Same as Figure 5.2, but with the data binned in a regular grid of points with an interval of 0.0048 days (6.8 min). The error bars are the standard deviation of the average divided by the square root of the number of points in the bin.

$v\sin i \leq$ 5 km/s, and a metallicity similar to that of the Sun. The slow rotation is particularly significant, for several reasons: it indicates that the star has not been spun up by tidal interactions with a massive secondary, it forecloses some blending scenarios, and it means that more precise radial velocity measurements can be obtained fairly readily.

5.4.1 A whole visible range spectrum

In order to confirm the photometric classification of the star, we also obtained a moderate-resolution echelle spectrum covering the entire visible wavelength range, using the Palomar 1.5 m telescope. Based on the comparison of this spectrum with the spectral standards of Montes et al. (1999), we classify the star as K0V. It shows no sign of a composite spectrum or of other peculiarities.

5.5 High signal to noise radial velocity observations

We obtained precise radial velocity measurements using the I_2 absorption cell and High Resolution Spectrometer on the Keck I telescope. Eight observations were collected over a period of 18 days in July 2004, providing good coverage of critical phases. The data reduction involved modeling of the temporal and spatial variations of the instrumental profile of the spectrograph (Valenti et al. 1995), and it is conceptually similar to that described by Butler et al. (1996). Internal errors were computed from the scatter of the velocities from the echelle

TABLE 5.2— Parameters for the TrES-1 Planet

Parameter	Value
	Orbital
P	$3.030065 \pm 8 \times 10^{-6}$ days
T_c	2453186.8060 ± 0.0002 (HJD)
a	0.0393 ± 0.0011 AU
i	$88.5^{+1.5}_{-2.2}$ deg
K	115.2 ± 6.2 m s^{-1}
	Physical
M_P	$(0.75 \pm 0.07) M_{Jup}$
R_P	$1.08^{+0.18}_{-0.04} R_{Jup}$
R_P/R_s	$0.130^{+0.009}_{-0.003}$

orders containing I_2 lines and are typically 10-15 m/s. Figure 5.4 shows the radial velocity measurements, along with a fit to a sinusoidal variation that is constrained to have a period and phase determined from the photometric data. This constrained fit matches the data well and yields a velocity semiamplitude of K = 115.2 ± 6.2 m/s. The rms residual of the fit is 14 m/s, in good agreement with the average of the internal errors. Examination of the spectral line profiles in our Keck spectra by means of the bisector spans (Torres et al. 2004a) indicated no significant asymmetries and no correlation with orbital phase, once again ruling out a blend.

5.6 Discussion

To provide an initial estimate of the planetary mass and radius, we used the main-sequence calibration from Cox (2000), and assumed that TrES-1 parent star is a K0V with solar metallicity, a mass M_s=0.80 $M_\odot$ and a radius R_s=0.86 $R_\odot$. We took limb darkening relations from Claret (2000) and from Claret (2004, private communication), for models with solar metallicity, log(g)=4.5, and T_{eff}=5250 K. We assign (somewhat arbitrarily) an uncertainty of ±0.07 $M_\odot$ to M_s. We also take $0.80_\odot \leq R_s \leq 0.95 R_\odot$, since adequate fits to the photometry cannot be obtained for stellar radii outside this range.

From the observed reflex stellar velocity and Kepler's laws, we estimated the semi-major axis a and the planetary mass M_p, using the constraints and assumptions just described. We then performed a minimum-χ^2 fit to all of the photometry (with errors estimated from the scatter of the input data), to obtain estimates on the planetary radius R_p and orbital inclination i, and to

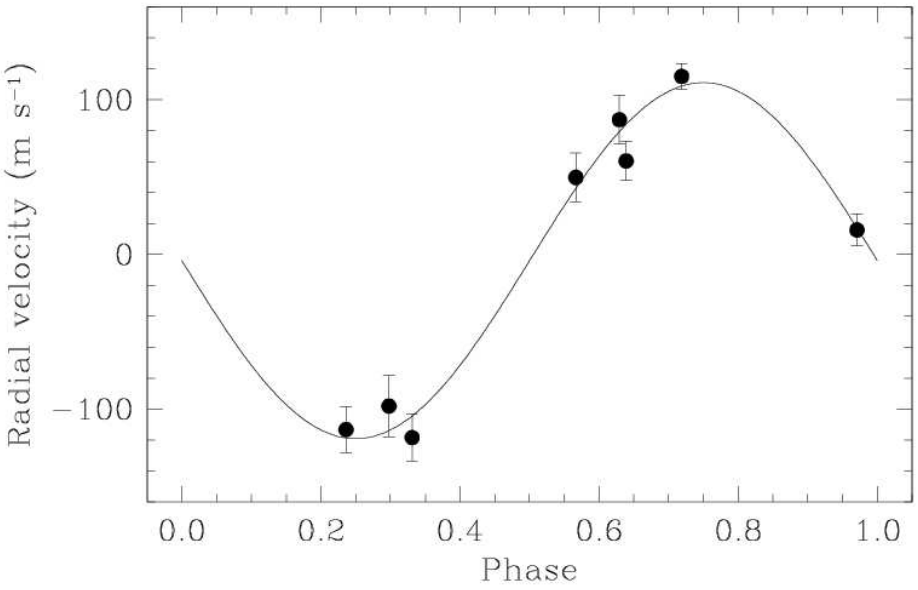

FIGURE 5.4— Keck I/HIRES radial velocity observations of TrES-1, overplotted with the best-fit orbit.

refine the estimates of the epoch of transit center T_c and the orbital period P. Our best estimates for the stellar, planetary and orbital parameters are given in Table 5.2, and the solid curves in Figures 5.1 and 5.4 show the fitted photometric and radial velocity variations overplotted on the data.

The error estimates given in Table 5.2 include errors that follow from our uncertainty in the radius and mass of the parent star (which is assumed to be a main-sequence object), as indicated in Table 5.1. These uncertainties (especially in R_s) dominate errors in the photometry as regards estimates of R_p and i. If the stellar radius and mass were known more accurately, the uncertainties in these parameters would be smaller by about a factor of 10. Contrariwise, if the star is actually a subgiant (photometric constraints notwithstanding), R_p could exceed the upper limit in Table 5.2. The error in M_p arises about equally from the radial velocity measurement precision and from our uncertainty in M_s.

The quantities in Table 5.2 allow us to estimate some further properties of the planet. We find the equilibrium surface temperature:

$$T_e = T_s(R_s/2a)^{1/2}[f(1-A)]^{1/4} = 1250(1-A)^{1/4} \tag{5.1}$$

where A is the Bond Albedo, and we assume efficient energy redistribution over

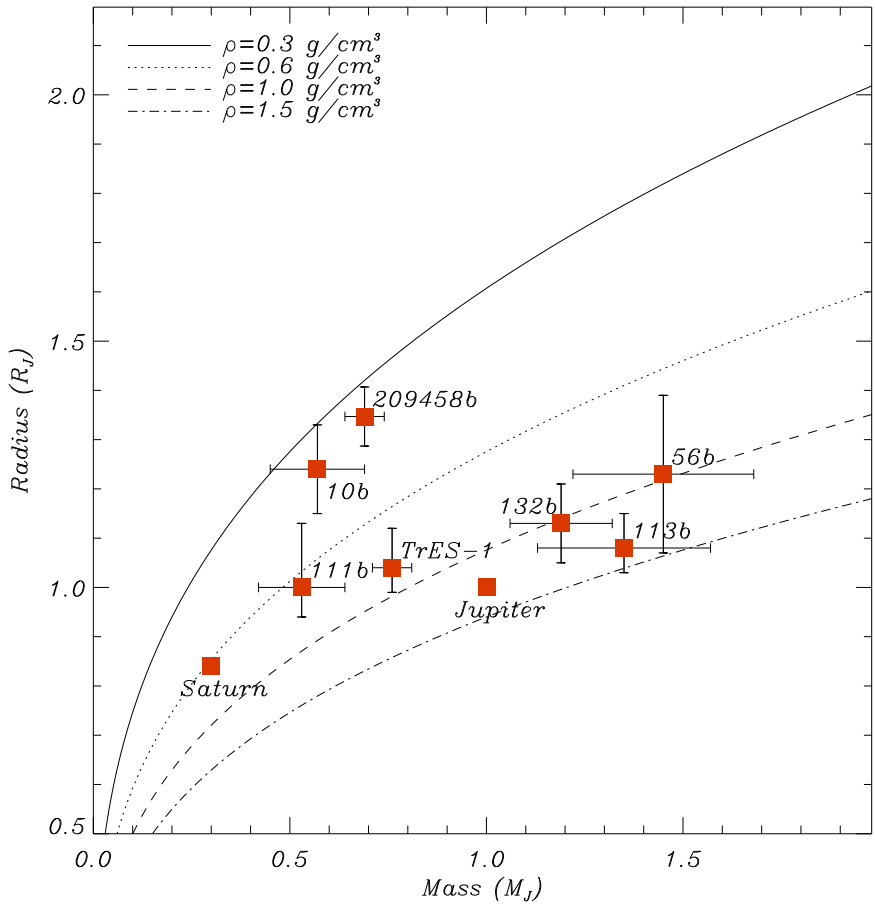

FIGURE 5.5— Radii of transiting extrasolar planets plotted against their masses. Dashed curves are lines of constant density. Data are from Brown et al. (2001) for HD 209458b, Torres et al. (2004a) for OGLE-TR-56b, Bouchy et al. (2004) for OGLE-TR-113b, Moutou et al. (2004) for OGLE-TR-132b, Pont et al. (2004) for OGLE-TR-111b, Konacki et al. (2005) for OGLE-TR-10b, and Sozzetti et al. (2004) for TrES-1.

the surface of the planet ($f = 1$). We also obtain the mean density 0.74 g/cm^3, the surface gravity 1373 cm/s^2, and the escape speed, v_e=47 km/s.

The mass, orbital radius, and radiative equilibrium temperature of TrES-1 are quite similar to those of HD 209458b, yet the former planet's radius is about 20% smaller. Indeed, as shown in Figure 5.5, the radius of TrES-1

is more similar to those of the OGLE planets, as it closely matches current models for irradiated planets without internal energy sources (Chabrier et al. 2004, Burrows et al. 2004). This discrepancy between the radii of HD 209458b and TrES-1 reinforces suspicion that HD 209458b has an anomalously large radius.

5.7 On-going and future works

To provide a better confrontation between theory and observation for this object, the stellar radius (and to a lesser degree, mass) could be better constrained. A more detailed analysis of the Keck spectra (Sozzetti et al. 2004) together with spectra obtained at the Hobby-Eberly Telescope allowed these authors to further constrain the stellar parameters of the TrES-1 Parent Star, deriving $T_{eff} = 5250 \pm 75$ K, $\log g = 4.6 \pm 0.2$ and [Fe/H] $= 0.00 \pm 0.09$, $M_s = 0.89 \pm 0.05 M_\odot$, $R_s = 0.83 \pm 0.05 R_\odot$. The star showed activity (measured by the Ca II indicator) and no Li down to the measurable level ($\log \epsilon(Li) < 0.1$), which led these authors to constrain the age of the system to the values 2.5 ± 1.5 Gyr. The improved planetary mass, radius and inclination of the orbit were:

- $M_p = 0.76 \pm 0.05\ M_J$
- $R_p = 1.04^{+0.08}_{-0.05}\ R_J$
- $i = 89.5^{+0.5}_{-1.3}$ degrees

5.7.1 HST observations

Additionally, we have undertaken a HST 15-orbit (3 visits of 5 orbits each) Director Discretionary's Time observing run on TrES-1, using the ACS/HRC with a grism. With this configuration, we estimate that we can achieve only a factor of 2.2 loss in precision with respect to the 40 times brighter HD 209458 star's photometry performed with STIS by Brown et al. 2001. This is mainly due to the much higher efficiency of the grism on ACS than the medium resolution STIS grating used in the HD 209458b case. With photometry of sufficient accuracy, it is possible to fit independently 4 key parameters of the star/planet system: the star radius, the planetary radius, the limb darkening coefficient and the orbital inclination. Although these refinements of the parameters (which are expected to reinforce the difference in radius of HD 209458b and TrES-1, thus providing a theoretical challenge for the explanation of the radii of the two objects) were the major objective of this run, there were also other by-products: these observations should allow for searches of few-earths sized hypothetical satellites (even if they are not expected due to the strong tidal

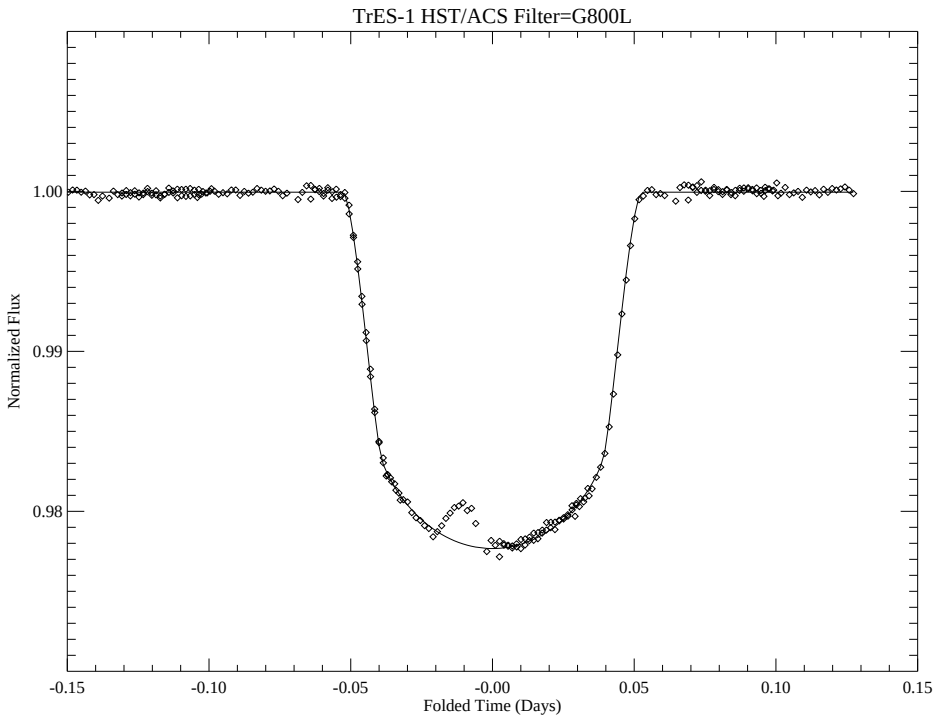

FIGURE 5.6— Preliminary HST/ACS light curve of TrES-1, showing a feature that can be interpreted as a spot being eclipsed by the planet.

forces in the close Hot Jupiter's orbits), either from residual photometric information of satellite's transits (constraining the satellite's size) or from the time-shift induced by the companion (constraining the satellite's mass; see, e.g. Sartoretti & Schneider 1999). Upper limits will be placed on the presence of opaque rings around the planet. With the data still under analysis, in Figure 5.6 we can advance a preliminary light curve. This shows an increase in brightness close to the center of the transit. This event was only observed in one of the three visits, and this phase of the transit was not observed again. There are two scenarios that could explain the presence of this feature: *i)* a big warm stellar spot (warm because otherwise there would be a color dependance of the feature that is not observed in this preliminary analysis), with a size of $\sim$1 R_J, being occulted by the planet, and *ii)* a hypothetical second planet in an outer orbit that would have been in transit at the moment that TrES-1 was in transit. The latter is a much more improbable explanation, as it works if

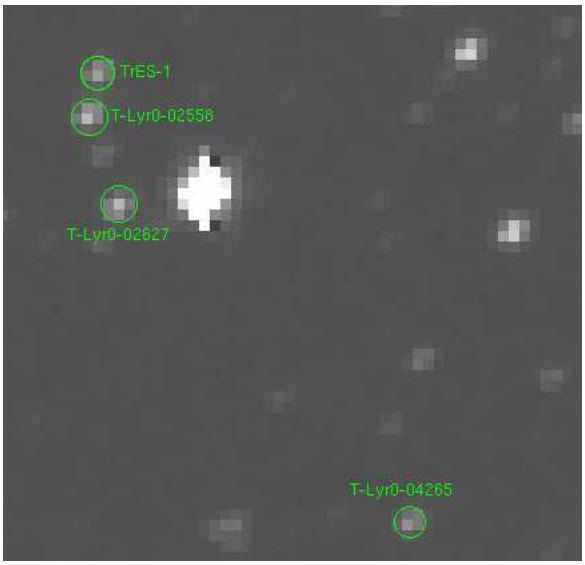

FIGURE 5.7— The location of TrES-1 and the three reference stars used to study its long term variability, summarized in Figure 5.8.

the planet is at a distance of roughly 1 AU. The chances to have observed this second planet in transit are thus quite low.

The presence of a spot in the HST data is not surprising, considering the known activity of the star, based on the Ca II indicator (Sozzetti et al. 2004). In order to establish if the activity of the star is detectable in the STARE data, we binned the raw light curve in 2 hour bins, whenever there were more than 50 data points inside each bin. To provide a comparison sample, we repeated the same operation in three close stars to TrES-1 (plotted in Figure 5.7), and estimated the standard deviation of each of the binned light curves. These plots are given in Figure 5.8, and the final standard deviation of the binned points for TrES-1 is larger by $\sim$24% than the mean standard deviation of the rest of the stars, that again points towards stellar activity on TrES-1 parent star.

5.7.2 Spitzer observations

With another experiment in a different wavelength range, we have pursued the detection of the TrES-1 planet secondary eclipse (the planet passing behind the host star), with the use of the IRAC detector on board the Spitzer Space Telescope. Even though there had been several attempts, only upper limits

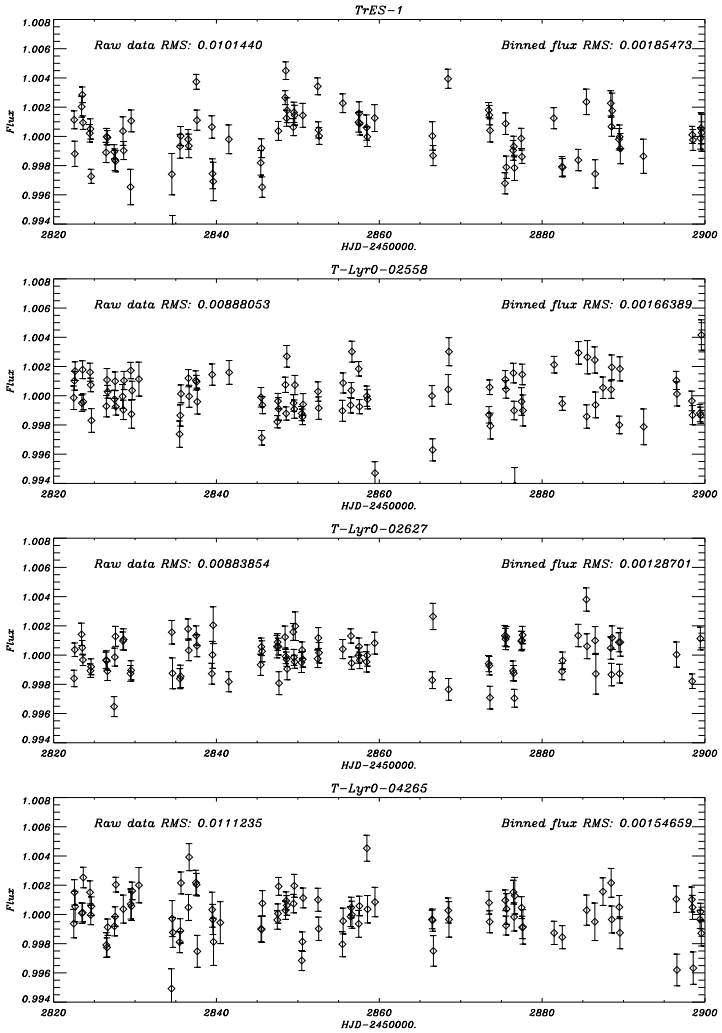

FIGURE 5.8— 2-hours binned light curves of TrES-1 and 3 close comparison stars with similar brightness (the location of the comparison stars is plotted in Figure 5.7). The error bars are the standard deviation of the data points inside each bin divided by the square root of the number of points. The RMS dispersion of the raw data is shown at the top left of each plot, and the dispersion of the binned light curves at the top right.

on the detection of thermal emission from an exoplanet have been published (Charbonneau et al. 1999; Collier Cameron et al. 2002; Leigh et al. 2003).

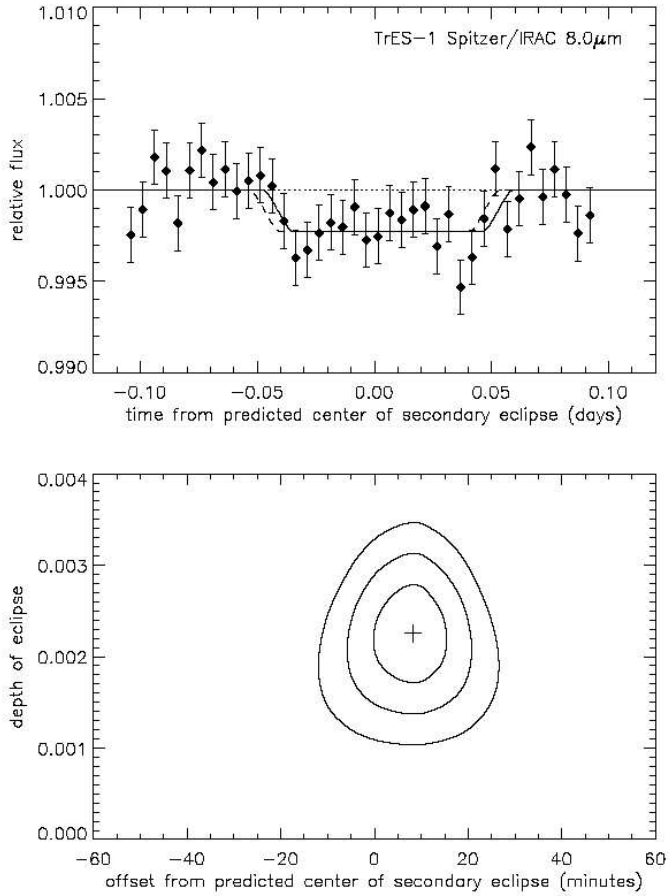

FIGURE 5.9— Upper panel: The binned 8.0 μm time series The best-fit model eclipse curve has a depth of ΔF=0.00225 and a timing offset of Δt=+8.3 minutes, and is plotted as the solid black line. A model of the same depth but Δt=0 is shown as the dashed line. Lower panel: The 1σ, 2σ and 3σ confidence ellipses on the eclipse depth and timing offset. From Charbonneau et al. (2005).

A second objective of these observations was to constrain the planetary orbit's eccentricity. A non-zero eccentricity detection could provide a mechanism for deposition of energy in the planet's interior (and thus increase its radius), a mechanism that has been proposed to explain the apparently anomalous radius of HD 209458b (Bodenheimer, Laughlin, & Lin 2003). The observations were carried during 5.6 hours on the night of Oct 30-31 2004, in two wavelength

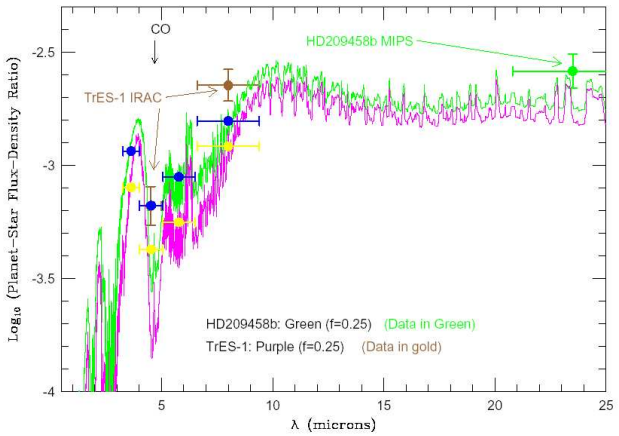

FIGURE 5.10— The logarithm base ten of the planet-to-star flux density ratio as a function of wavelength for the models of Burrows, Hubeny, & Sudarsky (2005) for TrES-1 (purple) and HD 209458b (green), assuming f=0.25 (a parameter that represents isotropic infrared emissions). Superposed are the secondary eclipse data: the gold dots with corresponding error bars are the TrES-1 data (Charbonneau et al. 2005), while the green dot with error bar is the HD 209458b data from Deming et al. (2005). From Burrows, Hubeny, & Sudarsky (2005).

bandpasses centered at 4.5 and 8 μm. The analysis revealed the first detection of thermal emission from an extrasolar planet[3] (Charbonneau et al. 2005), with a 6-σ detection of the secondary at 8 μm (Figure 5.9), and a 5-σ detection at 4.5 μm. The observed depths are 0.00225$\pm$0.00036 and 0.00066$\pm$0.00013, respectively. Under the assumption that the planet emits as a blackbody, the effective temperature of the planet is estimated as T_p=1060$\pm$50 K. There is no significant eccentricity detected, which forecloses the scenario proposed by Bodenheimer, Laughlin, & Lin (2003) for this planet. The same conclusion was obtained by Deming et al. (2005) for HD 209458b. If the planet is assumed to emit isotropically, then the implied Bond albedo is A=0.31$\pm$0.14. A comparison of these results with published models of planetary thermal emission (Sudarsky, Burrows, & Hubeny 2003) indicates that the measured flux at 4.5 μm might be explained by CO absorption (see Figure 5.10), while the absolute level of the 8 μm data point might be due to water absorption (Burrows, Hubeny, & Sudarsky 2005).

[3]There is another simultaneous detection by Deming et al. (2005) of the secondary eclipse of HD 209458b at 25 μm, also with Spitzer

In this Chapter we have described the observations that led to the discovery of the transiting planet TrES-1, which, at the moment of writing these lines, remains as the second better known exoplanet. The precision on its orbital and physical parameters is at the level of the planet orbiting the brighter star HD 209458. Its brightness in the infrared has made it possible to detect the secondary eclipse, and thus, thermal emission from an exoplanet. This detection provided the effective temperature of the planet, and it gives clues, according to some authors, for a tentative detection of CO and water absorption in its atmosphere. It does also argue against a proposed mechanism for energy deposition in the interior of the planet, which does not seem to be taking place in the bigger HD 209458b planet either. More transiting planets and theoretical effort are needed to understand the sizes of these objects. This implies adding more points in the Figure 5.5. In the next Chapter, we apply the technique for exoplanetary atmospheres investigation called transmission spectroscopy to the 2004 Venus transit. This technique will help to study the atmospheres of the newly found transiting planets.